

Research Article

Open Access



# Printed graphene/CNTs/TPU-fabric wearable strain sensor for healthcare monitoring

Weikai Zhao<sup>1</sup>, Pei He<sup>1,\*</sup>, Kai Ling<sup>1</sup>, Chen Gao<sup>1</sup>, Kaifeng Wang<sup>2</sup>, Lin Wu<sup>1</sup>, Junliang Yang<sup>2,3,\*</sup>

<sup>1</sup>School of Electronic Information, Central South University, Changsha 410083, Hunan, China.

<sup>2</sup>Hunan Key Laboratory for Super-microstructure and Ultrafast Process, School of Physics, Central South University, Changsha 410083, Hunan, China.

<sup>3</sup>FuRong Laboratory, Changsha 410078, Hunan, China.

**\*Correspondence to:** Dr. Pei He, School of Electronic Information, Central South University, 932 Lushan South Road, Changsha 410083, Hunan, China. E-mail: pei.he@csu.edu.cn; Prof. Junliang Yang, Hunan Key Laboratory for Super-microstructure and Ultrafast Process, School of Physics, Central South University, 932 Lushan South Road, Changsha 410083, Hunan, China. E-mail: junliang.yang@csu.edu.cn

**How to cite this article:** Zhao, W.; He, P.; Ling, K.; Gao, C.; Wang, K.; Wu, L.; Yang, J. Printed graphene/CNTs/TPU-fabric wearable strain sensor for healthcare monitoring. *Soft Sci.* 2025, 5, 10. <https://dx.doi.org/10.20517/ss.2024.61>

**Received:** 31 Oct 2024 **First Decision:** 25 Nov 2024 **Revised:** 1 Jan 2025 **Accepted:** 2 Jan 2025 **Published:** 6 Feb 2025

**Academic Editors:** Seung Hwan Ko, Carlo Massaroni **Copy Editor:** Ting-Ting Hu **Production Editor:** Ting-Ting Hu

## Abstract

Wearable strain sensors hold immense promise in monitoring human motion activities due to their low cost, lightweight design, and excellent biocompatibility. For example, continuous real-time monitoring of neck activity can effectively prevent the onset of acute torticollis. However, current approaches to monitoring sleep neck posture primarily depend on technologies such as computer vision, which are characterized by limited wearability and portability issues. Herein, this work introduces a cost-effective, highly sensitive carbon-based strain sensor fabricated on a fabric substrate with a printing technique, which is eco-friendly and biocompatible. The proposed sensor displays a broad sensing range of 112%, high sensitivity (gauge factor > 210), low sensing limit (~ 0.1  $\mu\text{m}$ ), and outstanding long-term stability over 3,000 cycles. The sensor's utilization in monitoring joint motion, vocal cord activity, pulse, and electrocardiogram (ECG) is illustrated. Moreover, a portable system for monitoring neck activity and ECG signals while sleeping has been engineered, capable of detecting neck movements and ECG signals during sleeping hours. The composite materials design strategy combined with printing techniques provides a potential route for high-performance and low-cost wearable strain sensors in health monitoring.

**Keywords:** Strain sensors, sleep posture monitoring, multimodal monitoring, wearable system



© The Author(s) 2025. **Open Access** This article is licensed under a Creative Commons Attribution 4.0 International License (<https://creativecommons.org/licenses/by/4.0/>), which permits unrestricted use, sharing, adaptation, distribution and reproduction in any medium or format, for any purpose, even commercially, as long as you give appropriate credit to the original author(s) and the source, provide a link to the Creative Commons license, and indicate if changes were made.



## INTRODUCTION

Torticollis, also known as wry neck, is characterized by a sudden injury or overuse of neck muscles or structures, resulting in neck pain and functional limitation<sup>[1]</sup>. Diagnosis of torticollis is currently centered on clinical evaluation, and computer vision and image recognition techniques have been applied to analyze postures and movements recorded by surveillance cameras or other imaging devices<sup>[2]</sup>. By identifying abnormal motion patterns in the head and neck area, indicators of torticollis can be detected. Additionally, specific wearable devices are capable of recording changes in head and neck positioning, aiding in the recognition of abnormal neck movements and possible torticollis cases while asleep<sup>[3]</sup>. As a key component of wearable devices, flexible sensors can react to external stimuli and have become a prominent research topic because of their distinctive performance benefits<sup>[4]</sup>, including low cost, lightweight design, and excellent biocompatibility<sup>[5-7]</sup>. These sensors hold significant application potential in areas such as electronic skin<sup>[8-10]</sup>, human-machine interaction<sup>[11-14]</sup>, and personal healthcare monitoring<sup>[15-19]</sup>. Furthermore, flexible sensors can more readily achieve close contact with human skin, thereby aiding in the reduction of environmental noise and enhancing the precision of physiological information detection.

Flexible strain sensors are typically made of conductive sensing materials and elastic substrates<sup>[20,21]</sup>. In contrast to traditional conductive materials, nano-scale conductive materials with superior electrical and mechanical properties are garnering increasing attention<sup>[22,23]</sup>. Two-dimensional (2D) graphene, noted for its exceptional properties, has been a catalyst for transformation across various industries<sup>[24,25]</sup>. Graphene, producible on a mass scale through chemical vapor deposition (CVD), serves as a cost-effective conductive material for sensors<sup>[4,26]</sup>. Graphene-based flexible strain sensors are known for their ultra-high sensitivity, attributed to the crack propagation mechanism<sup>[27]</sup>; however, they typically exhibit suboptimal tensile properties<sup>[28]</sup>. Incorporating high-aspect-ratio carbon nanotubes (CNTs) can enhance the sensing range, yet CNTs-based strain sensors often demonstrate low sensitivity, as the conductive network remains stable even at elevated strain levels<sup>[29]</sup>. Thus, integrating graphene with CNTs effectively balances the fundamental sensing performance of strain sensors.

Fabrics, with their softness, stretchability, and porosity derived from high-aspect-ratio fibers, are among the most common and adaptable materials. The interlaced fiber structure endows fabrics with flexibility, breathability, and comfort. Incorporating sensing units into fabrics used in daily personal items can readily fulfill the fundamental requirements of wearable technology without causing significant discomfort to the human body<sup>[7,30,31]</sup>. Consequently, fabrics are gaining significant attention as promising substrate materials for wearable healthcare sensor devices<sup>[32]</sup>. Given the inherent properties of fabrics (e.g., roughness, porosity, and hygroscopicity), developing flexible fabric-based electronic devices presents numerous challenges. Reports indicate that researchers commonly employ the following strategies to address the manufacturing challenges of fabric-based electronic products. Initially, conductive fibers can be integrated into the fabric in a manner that ensures sensing capabilities and wearability without compromising its performance and aesthetics<sup>[33,34]</sup>. However, the porous, rough, and hygroscopic nature of fabrics can lead to uneven distribution of sprayed conductive films, potentially diminishing electrical performance<sup>[35]</sup>. Moreover, the conductive film is susceptible to damage due to fiber movement throughout the stretching process. Additionally, the low adhesion between the conductive material and the fabric<sup>[36]</sup> necessitates a passivation layer to avoid delamination or peeling of the film on the fabric.

At present, the adoption of flexible wearable strain sensors remains limited. Thus, while ensuring the sensor's high performance, advancing a scalable, cost-effective manufacturing process is essential for fostering its commercialization. The printing process has become a trusted solution for manufacturing a range of flexible devices, citing its high efficiency, cost-effectiveness, and versatility in patterning<sup>[37-39]</sup>.

Nonetheless, utilizing certain raw materials in device fabrication presents potential risks to both the environment and human health. The solvent-based preparation process offers a cost-effective approach to sensor manufacturing; however, it involves the use of organic solvents that can be detrimental to human health and the environment<sup>[40,41]</sup>.

Herein, we present an environmentally friendly and biocompatible carbon-based strain sensor that is simple, cost-effective, and highly performant. By utilizing the green solvent dihydrolevoglucosenone (Cyrene), the thermoplastic polyurethane (TPU), graphene and CNTs were dispersed in the solvent to formulate a printable conductive ink. Subsequently, the strain sensor was fabricated by applying the ink onto elastic fabric via the printing process, and its exceptional sensitivity and long-term stability were evaluated. It showcased applications in monitoring joint bending, laryngeal phonation, pulse, and electrocardiogram (ECG). Ultimately, a wearable system for monitoring neck movement and ECG signals while sleeping was engineered, capable of detecting neck motion and ECG signals throughout sleep.

## EXPERIMENTAL

### Materials

Graphene powder (Oxygen content  $\leq 0.01$  wt%, Carbon  $\geq 99$  wt%, diameter: 15–25  $\mu\text{m}$ ) was sourced from DT NANOTECH Inc., China. CNTs (Whisker-CNT0076G, purity: 95%, diameter: 10–30  $\mu\text{m}$ ) were procured from Jiangxi Kelaiwei Carbon Nano Materials Co. Ltd. TPU powder [density: 1.20 g/cm<sup>3</sup>, granular size distribution (GSD): 0–80  $\mu\text{m}$ ] was sourced from Bayer Co., Ltd. Cyrene (C<sub>6</sub>H<sub>8</sub>O<sub>3</sub>) was sourced from Sigma-Aldrich Trading Co., Ltd., Shanghai, China. Heat transfer (HT) paper was sourced from Transmax, USA. All materials were utilized in their as-received state without undergoing any additional purification.

### Preparation of graphene-CNTs-TPU composited ink

In summary, 2 g of TPU powder was combined with Cyrene (20 mL) and a minor quantity of fluorosurfactant (0.2 wt%, Capstone FS-3100, Du Pont Co., Ltd), and then the TPU-Cyrene mixture was homogenized under vacuum in a defoaming apparatus at a high rotational speed of 3,000 revolutions per min (rpm) for 10 min by a speed mixer (SIE-MIX80, Guangzhou SIENOX Technology Co., Ltd., China). Once cooled, 1g of CNTs was introduced, and the mixture was stirred at 3,000 rpm for 5 min. Subsequently, an equivalent mass of graphene was added, stirred at 3,000 rpm for 3 min, and then cooled for 6 min. The stirring and cooling cycle was repeated 3 times, and ultimately, the graphene-CNTs-TPU conductive ink was produced.

### Fabrication of graphene-CNTs-TPU/fabric composite strain sensor

The conductive ink exhibits strong adhesion to HT paper, satisfying the printing requirements for extensive patterns<sup>[42]</sup>. Once the elastic fabric and HT paper were trimmed to the appropriate size, the highly elastic bottom layer of the HT paper was detached from the backing sheet. The HT paper was smoothly aligned on the fabric and then both were positioned on the HT machine workstation, subjected to pressure at 170 °C for 10 s with a substantial force, and ultimately, the elastically enhanced decorated fabric was achieved. The composite ink was applied to the decorated fabric using the stencil printing method and then cured in an oven at 80 °C for 150 min, yielding a graphene-CNTs-TPU composite film with dimensions of 25 mm<sup>2</sup> × 4 mm<sup>2</sup>. Ultimately, the film was cut into strip-shaped strain sensor devices, with dimensions of approximately 27 mm<sup>2</sup> × 8 mm<sup>2</sup>.

### Characterization and measurement

Strain sensing tests were performed on a linear test bench that incorporates a tension control system. The ends of the strain sensor were secured in the stretching test machine (FlexTestS-P2, Hunan NanoUp Electronics Technology Co., Ltd., China) and connected to a source meter (Keithley-2400, Tektronix Inc.,

USA) to track resistance changes. The surface topography of the strain sensor was analyzed using a field-emission scanning electron microscope (SEM, JEOL, Japan) with an accelerating voltage of 10 kilovolts (kV). The impedance data was obtained using a LCR meter (HTOKI-IM3536, Hioki E.E. corporation, Japan). Human motion and health-related data were gathered using a portable digital measurement device (01RC, Hangzhou LinkZill Technology Co., Ltd, China). ECG monitoring was achieved using a miniature digital ECG development board (WDECG), which integrates ECG signal acquisition, processing, and wireless transmission. A sleep monitoring system was developed to enable real-time measurement of both neck posture while sleeping and the associated ECG signals.

## RESULTS AND DISCUSSION

### Structure and sensing properties of strain sensor

**Figure 1A** depicts the manufacturing process of the graphene-CNT-TPU/fabric strain sensor. **Figure 1B** displays the final sensor, notable for its compactness, rendering it appropriate for a range of human monitoring applications. The fibrous structure of the elastic knit fabric [**Figure 1C**] and the smoothness of its fiber surface attest to the fabric's superior elasticity and structural stability. The surface morphology of the HT paper [**Figure 1D**] reveals a clearly defined porous structure, which enables the conductive ink to partially infiltrate the HT paper, thereby strengthening ink adhesion during printing. **Supplementary Figure 1** illustrates the process of attaching transfer paper to the modified fabric using a heat press, culminating in the modified fabric as depicted in **Supplementary Figure 1B**. **Supplementary Figure 2** demonstrates the performance characteristics of the graphene-CNT-TPU ink. When the ink is applied to the HT paper-modified fabric, it creates a composite film on the fabric's surface, as depicted in **Figure 1E**, displaying a markedly uneven and porous structure. As seen in **Figure 1F** and **Supplementary Figure 3**, TPU encapsulates the graphene surface in an irregular pattern, harboring numerous CNTs. The bridging CNTs link disparate graphene sheets, significantly enhancing the conductivity network and boosting the film's conductivity and sensing stability. **Supplementary Figure 4A (i)** and **(ii)** shows the dual-layer structure of the HT paper and its adherence to the fabric. **Supplementary Figure 4B (i)** indicates that the boundary between the composite film and the HT paper coating is indistinct. The sensor's cross-section substantiates the non-uniformity of the composite film surface [**Supplementary Figure 4B (ii)**].

To investigate the impact of HT paper and various elastic fabrics on the strain sensing range and sensitivity of graphene-CNTs-TPU composite films, three types of sensors were fabricated using the same conductive ink: one on ultra-elastic fabric with HT paper decoration (Sensor I), one on a cleanroom wiper with HT paper decoration (Sensor II), and one on untreated ultra-elastic fabric (Sensor III). **Figure 2A** illustrates the impact of HT paper and various fabrics on sensor performance. In comparison to Sensors I and III, the fabric adorned with HT paper significantly enhances the strain-sensing range of the graphene-CNTs-TPU composite film over that of the untreated fabric. Notably, Sensor III possesses only approximately 8% of the maximum sensing range. Given that when conductive ink is directly printed onto the fabric, the majority adheres to the fiber's outer surface, with only a minor portion infiltrating the interior via the parallel gaps between fibers, and the fiber junctions remain largely ink-free. During the stretching of the fabric, micro-cracks form within the composite film when subjected to a force aligned with the fiber deformation direction, causing a significant rise in the resistance of Sensor III. Should the conductive network be entirely compromised, Sensor III forfeits its sensing capabilities entirely. When contrasting Sensor I with Sensor II, it is evident that opting for a fabric with greater stretchability substantially improves the strain-sensing range of the composite film. Given that the fibers of the cleanroom wiper are less dense than those of the ultra-elastic fabric, the gap expansion between the cleanroom wiper fibers during stretching is prone to causing HT paper rupture, consequently impacting the strain sensing range of the composite film. **Supplementary Figure 5** indicates that fabric selection exerts minimal influence on the composite film's sensitivity at low strain levels.



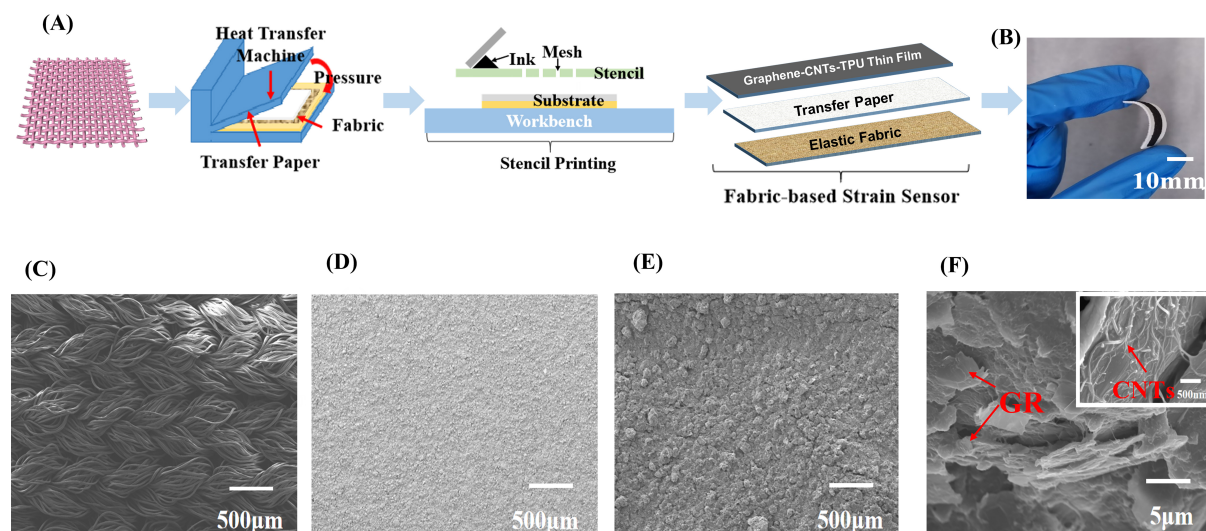


**Figure 1.** Fabrication process and microscopic SEM characterization of the sensor. (A) Schematic illustration of the fabrication process of the graphene-CNTs-TPU/fabric strain sensor; (B) Photograph of the sensor; (C) SEM characterization of the fabric; (D) SEM characterization of the HT paper; (E) SEM characterization of the composite film; (F) SEM characterization of the composite film at a high magnification ratio. SEM: Scanning electron microscope; CNTs: carbon nanotubes; TPU: thermoplastic polyurethane; HT: heat transfer; GR: graphene.

From the analysis above, it is evident that Sensor I exhibits superior performance. Consequently, all subsequent performance evaluations concentrate on this graphene-CNTs-TPU/fabric strain sensor. The sensitivity of this fabric-based strain sensor throughout the tensile process was systematically examined [Figure 2B]. Typically, sensitivity performance is assessed using the gauge factor (GF), defined by  $GF = (\Delta R/R_0)/\epsilon$ , where  $\Delta R$  represents the change in resistance during stretching,  $R_0$  is the initial resistance, and  $\epsilon$  is the applied strain. Notably, the sensor demonstrates high stretchability (reaching up to 112%), excellent sensitivity ( $GF > 210$ ), and good linearity ( $R^2 = 0.993$ ). The increase in GF is potentially associated with the microcrack formation and the variation mechanism within the graphene-CNTs-TPU composite film. [Supplementary Figure 6A](#) indicates that the strain sensor reacts at a motion state of 0.01 mm/s, correlating to an extremely low sensing threshold ( $\sim 0.1\%$ ), showcasing its ability to detect minute strains. [Supplementary Figure 6B](#) presents the I-V characteristic curves of the graphene-CNTs-TPU composite film. Evidently, a strong linear correlation between current and voltage is observed for the sensor across various stretch strain amplitudes. This suggests the consistent stability of the conductive network throughout stretching, essential for maintaining stable electrical output.

To further assess the reliability of the graphene-CNTs-TPU composite film strain sensor across various strain amplitudes, cyclic tensile testing was conducted at a constant frequency with varying amplitudes once the sensor reached a stable state. The response curve depicted in [Figure 2C](#) illustrates distinct responses to varying strain amplitudes. Under identical tensile amplitudes, each cycle exhibits excellent consistency, with responses being symmetric during both loading and unloading phases. Subsequently, a staircase-like strain was imposed on the sensor. [Supplementary Figure 7](#) shows the resistance variation of the sensor under varying degrees of tensile strain within a single cycle. Observations reveal that the sensor demonstrates excellent discrimination for varying strains, highlighting its ability to effectively detect multiple levels of tensile strain. [Supplementary Figure 8](#) indicates that the  $R/R_0$  ratio increases (decreases) in a stepwise manner throughout the incremental loading-holding (unloading-holding) cycles. To determine the stability of the graphene-CNTs-TPU/fabric strain sensor at various stretching velocities, cyclic tensile tests with a 20% strain amplitude at five distinct frequencies were executed, assuming stability. As illustrated in

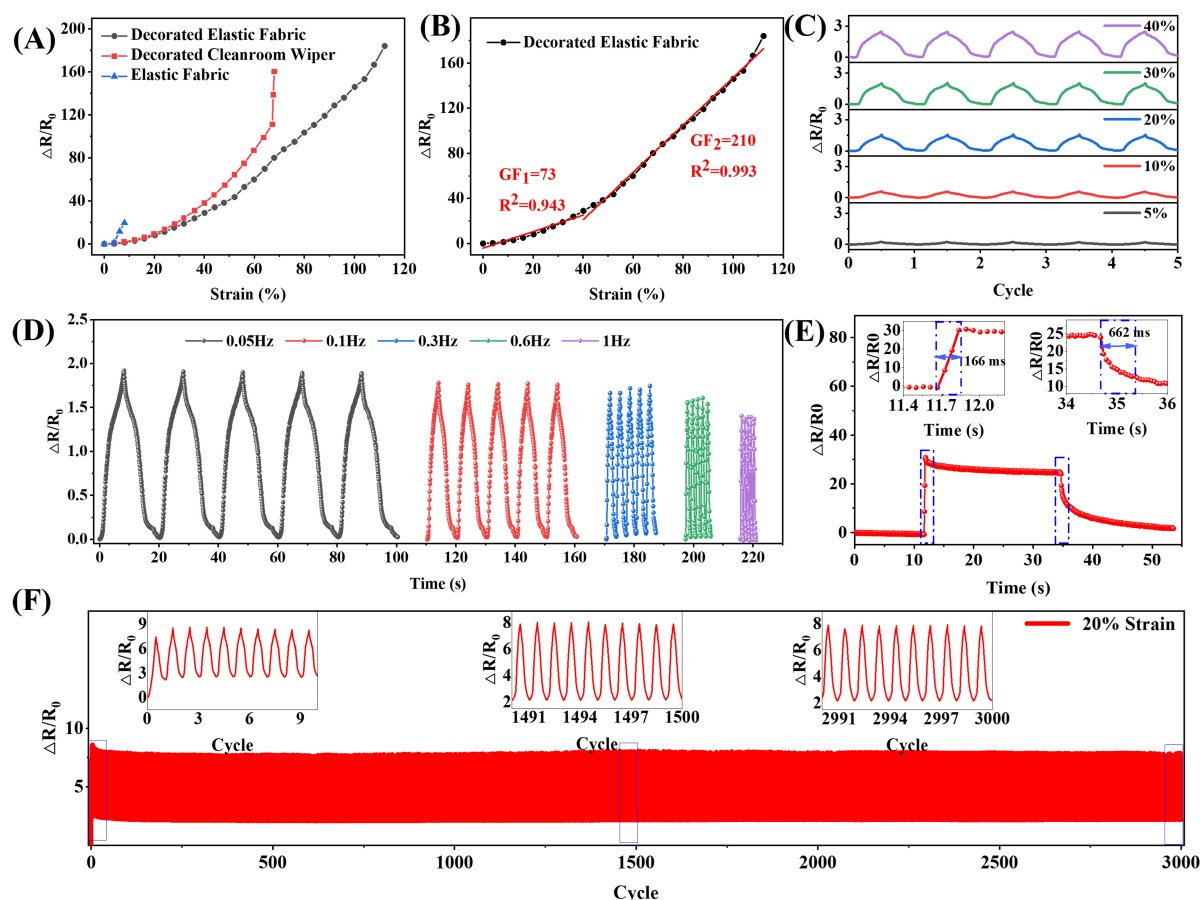


**Figure 2.** The characterization of sensor performance. (A) Response curves of sensors with conductive ink printed on ultra-elastic fabric decorated with HT paper, cleanroom wiper decorated with HT paper and untreated ultra-elastic fabric; (B) Strain sensing range, sensitivity and linearity of graphene-CNTs-TPU/fabric flexible strain sensor based on ultra-elastic fabric decorated with HT paper; (C) The cyclic responses of the stabilized sensor were measured under various strains at a frequency of 0.1 Hz; (D) The relative resistance of the stabilized sensor was observed during cyclic stretching at a strain of 20% across frequencies ranging from 0.05 to 1 Hz; (E) The tensile and recovery response times under a 5% strain were 166 and 662 milliseconds, respectively; (F) Long-term stability was assessed through durability testing of the graphene-CNTs-TPU strain sensor at a tensile rate of 0.5 mm/s over 3,000 cycles. HT: Heat transfer; CNTs: carbon nanotubes; TPU: thermoplastic polyurethane.

Figure 2D, the sensor's response is marginally influenced by the varying stretching speeds, potentially due to the suboptimal recovery characteristics of HT paper. The prolonged unloading response time causes the sensor's resistance to re-enter the loading phase prior to full recovery, resulting in an elevation of  $R_0$  and a reduction in the  $R/R_0$  value. Consequently, various loading-unloading frequencies exert a definite impact on the graphene-CNTs-TPU/fabric strain sensor.

Figure 2E shows that the loading response time and unloading response time of the sensor are 166 and 662 milliseconds, respectively, at a 5% strain after stabilization. The millisecond-level response speed ensures effective operation of the sensor at high stretching velocities. To determine the strain sensor's durability, its performance over 3,000 loading-unloading cycles at a 20% strain was evaluated. Figure 2F demonstrates that the relative resistance gradually decreases until it stabilizes. During the sensor's initial operational phase, the response peak value for the second cycle being higher than that of the first cycle could be attributed to more extensive microcrack formation following two stretching instances. Supplementary Figure 9 illustrates the differences among the response curves of four distinct cycles, showing that the curves for the 1,000 and

3,000th cycles are essentially superimposable. [Supplementary Figure 10](#) demonstrates the mechanical performance of the sensor. Following 1,000 cycles of bending, the sensor exhibited consistent resistance variation across cycles, demonstrating its excellent mechanical characteristics.

### Sensing mechanism analysis

To further elucidate the intrinsic mechanisms behind the electrical conductivity and tensile properties of the graphene-CNTs-TPU/fabric strain sensor, scanning electron microscopy (SEM) was utilized to characterize the sensor's morphological changes throughout the stretching process. [Figure 3A \(i\) and \(ii\)](#) displays the microscopic morphology of the sensor in its pristine state (0% strain). The surface of the composite film is devoid of any significant cracks and holes, characterized primarily by its texture. As the strain increases to 20%, incipient microcracks become visible on the surface, with widths measuring approximately 21.7  $\mu\text{m}$  [[Figure 3B \(i\) and \(ii\)](#)]. The stretching process causes the composite film to become thinner and narrower, and compression by stress along the z-axis leads to a reduction in the gap between internal conductive particles. The reduced spacing enhances the tunneling effect, thereby mitigating the impact on sensor resistance from microcrack formation and the relative displacement of graphene and CNTs. Upon reaching a 40% strain, the microcrack width expands to approximately 97.2  $\mu\text{m}$  [[Figure 3C \(i\) and \(ii\)](#)]. The predominant crack propagation mechanism leads to a marked increase in sensor resistance. Subsequently, the stress is relieved, and the sensor reverts to its original length [[Figure 3D \(i\) and \(ii\)](#)]. Compared to the initial state, it is evident that the microcracks on the composite film's surface do not fully close, with a remaining width of approximately 55  $\mu\text{m}$ . [Figure 3E](#) delineates this dynamic process into three distinct stages: the initial formation of microcracks (0% to 20%), the subsequent expansion of microcracks (20% to 40%), and the recovery phase of microcracks (40% to 0%). These surface micro-dynamic processes elucidate the phenomenon of gradually increasing resistance during the stretching process. Furthermore, the persistence of microcracks after the sensor is restored to its original length substantiates that the resistance is higher than that of the unstretched state. A small number of unsealed micro-cracks are visible on the surface, with the greatest crack width not surpassing 20 micrometers ( $\mu\text{m}$ ) after 3,000 stretching cycles [[Supplementary Figure 11](#)]. This observation attests to the composite film's structural integrity, securing the sensor's reliability.

### Application of human activities and healthcare monitoring

The graphene-CNTs-TPU/fabric strain sensor demonstrates high sensitivity, a low detection threshold, outstanding durability, and responsive symmetry, providing a clear advantage in the realm of human monitoring applications. [Figure 4A-D](#) illustrates the relative resistance changes as the strain sensor is affixed to various joints and flexed at multiple angles. Based on the specific shape and dimensions of the joint, strain sensors of varying sizes can be fabricated to facilitate bending monitoring. The results demonstrate that the response signal range varies with different joint bending angles, highlighting the sensor's application potential in auxiliary training and motion recognition applications.

The sensor's sensitivity to subtle vibrations was investigated. Initially, the sensor was affixed to the larynx and linked to an integrated wireless testing system to detect subtle variations in laryngeal muscles during vocalization. [Figure 4E, F](#) and [Supplementary Figure 12](#) display the sensor's responses upon repeating "Bye", "Hello", "Goodbye", and "Good Morning", respectively. These results demonstrate that the sensor is sensitive to laryngeal muscle vibrations and exhibits a consistent response to the same word or phrase. For words with varying numbers of syllables, the response exhibits a degree of differentiation. Subsequently, a simple wireless pulse monitoring system was assembled by positioning sensors over the radial artery and incorporating a wireless measurement and transmission system [[Figure 4G](#)]. As depicted in [Figure 4H](#), the pulse beat elicits a specific response from the sensor. The illustration reveals that the response features distinctive characteristic peaks, aligning with the known peaks of "Blow Wave P", "Tide Wave T", and

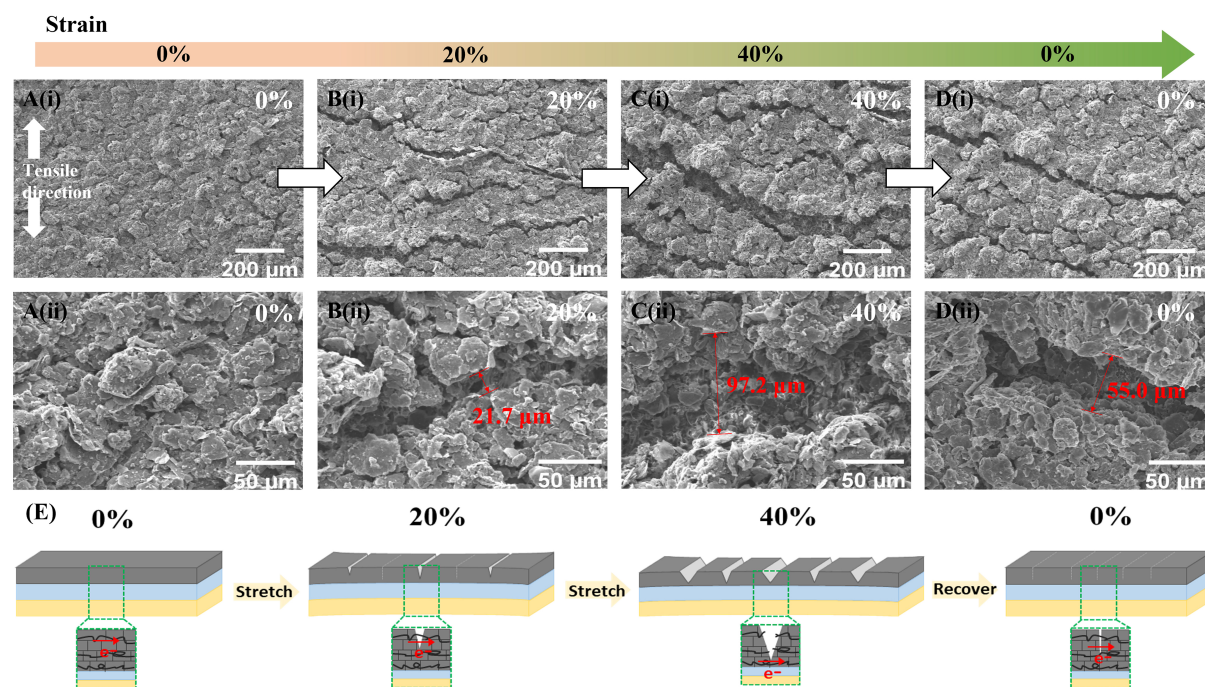


**Figure 3.** SEM images of the graphene-CNTs-TPU strain sensor at various stretching states during the first stretching/releasing cycle: A (i) and A (ii) 0%; B (i) and B (ii) 20%; C (i) and C (ii) 40% and back to D (i) and D (ii) 0 %; (E) Diagram of the stretching/releasing process. SEM: Scanning electron microscope; CNTs: carbon nanotubes; TPU: thermoplastic polyurethane.

“Diastolic Wave”, suggesting the sensor’s potential for pulse monitoring. Overall, the graphene-CNTs-TPU/fabric strain sensor offers practical utility in the realm of human micro-strain monitoring.

Additionally, to investigate the potential application of the graphene-CNTs-TPU composite film in healthcare monitoring, a composite film of appropriate dimensions [as depicted in [Supplementary Figure 13A](#)] was utilized as electrodes for ECG monitoring. The electrodes were affixed to the left and right arms, respectively, to interface with the ECG monitoring system [[Supplementary Figure 13B and C](#)]. For comparative purposes, a set of commercial Ag/AgCl electrodes were positioned similarly for ECG monitoring. Examination of [Figure 4I](#) reveals that the heart rates, determined by counting the peaks of the ECG waveform over a set interval, are approximately 65 bpm (black curve) and 78 bpm (red curve). [Supplementary Figure 13D](#) displays distinct P waves, QRS complexes, and T waves in both ECG signals, demonstrating that each signal accurately reflects the variations in electrical activity throughout the cardiac cycle. Comparative analysis of the ECG signals validates that the graphene-CNTs-TPU/fabric flexible electrode matches the performance of commercial Ag/AgCl electrodes in ECG monitoring. Further investigation of its conductivity revealed a square resistance of 172  $\Omega/\text{sq}$ , which is considered good, supporting the use of the electrode for ECG signal detection. [Supplementary Figure 14](#) illustrates the surface impedance of the electrode across various electrical signal frequencies. Consequently, this flexible electrode can be integrated directly into the wristband’s lining to create a wearable ECG monitoring platform.

### Sleep posture monitoring

Sleep posture variations, particularly of the neck, have a profound impact on sleep quality. Keeping the neck in a neutral alignment while supine can enhance good sleep quality. Utilizing a suitable pillow that supports the head and neck, aligning naturally with the spine, can significantly reduce neck stress and discomfort, aiding in the alleviation of neck pain and stiffness. Inappropriate pillow height or erroneous sleeping



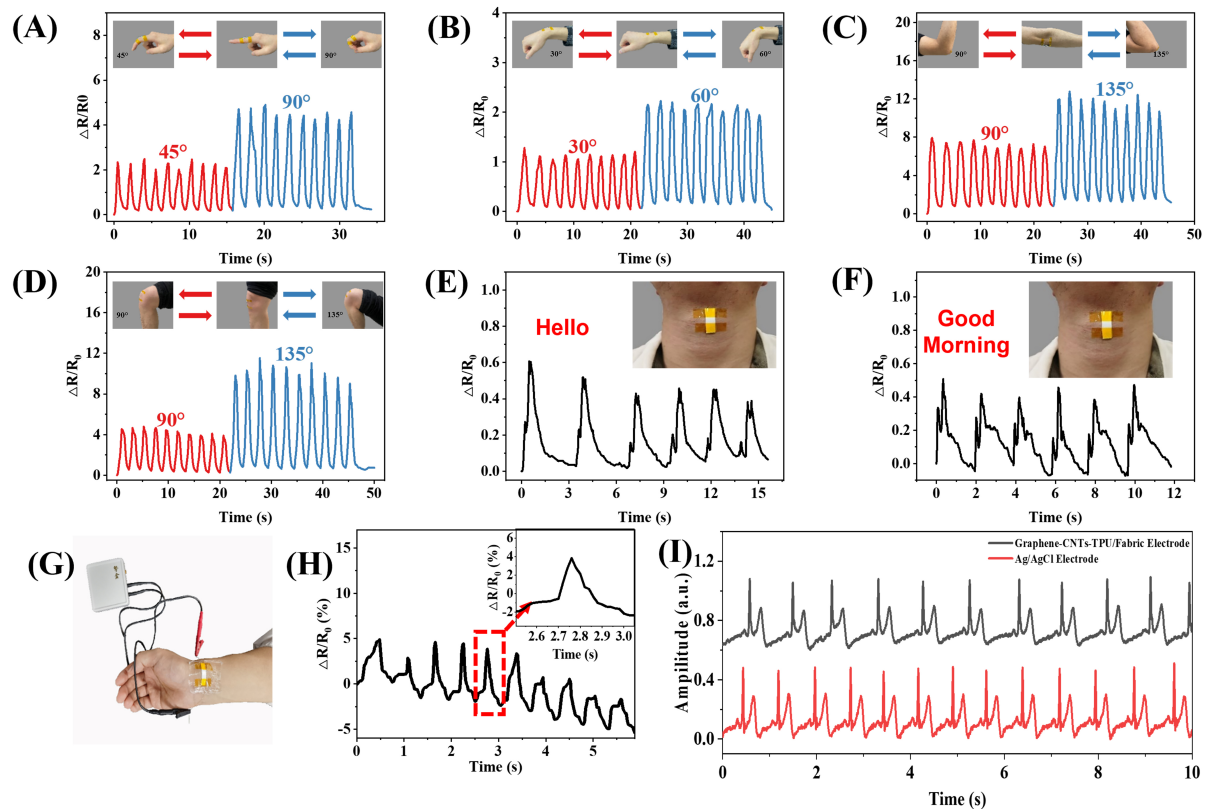


**Figure 4.** Human application testing of the sensor. (A–D) Relative resistance variety of the fabric strain sensor fixed on finger, wrist, elbow and knee joint; (E) Response signals recorded during speaking “Hello” and (F) “Good morning” respectively; (G) Photography of the strain sensor attached to the wrist and connected to a wireless monitoring system; (H) pulse monitoring. Illustration: The resistance signal of one pulse beat; (I) ECG signals obtained from the graphene-CNTs-TPU/fabric electrodes and Ag/AgCl electrodes. ECG: Electrocardiogram; CNTs: carbon nanotubes; TPU: thermoplastic polyurethane.

postures, such as using a pillow that is overly high or low, or having excessive head rotation or an unnatural angle, can cause intense pressure and distortion to the cervical spine. This may result in the overextension or torsion of neck muscles and ligaments, causing inflammation and pain. Furthermore, this can impair blood circulation in the neck, potentially causing muscle spasms and a sensation of rigidity. Hence, monitoring cervical spine posture fluctuations during sleep is essential. To tackle this issue, we have engineered a portable device that monitors neck posture and ECG signals during sleep.

Figure 5A displays the various common sleep positions. In the supine position, the head can be positioned straight up, turned towards the left, or turned towards the right, among other fundamental positions. Variations in head rotations lead to corresponding movements of the neck muscles. By tracking the twisting of the neck muscles, the sleeping posture can be identified. Figure 5B presents the system’s hardware circuitry. Supplementary Figure 15A and B shows the printed circuit board (PCB) layout and the schematic diagram of the circuit. Figure 5C features a photograph of the wearable device positioned on the neck. Figure 5D displays the actual design of the wearable device. Two strain sensors are attached to the wearable device for measuring the strain in the neck muscles. When the neck twists, it subjects the neck muscles to tension, which in turn induces a certain degree of strain in the sensors. Real-time cardiac monitoring during sleep is conducted by capturing the ECG signal from the carotid arteries or chest. Deviations in heart rate or ECG from the normal parameters can be immediately identified by healthcare professionals or family members via a mobile phone. Figure 5E provides an overview of the system diagram. The ECG sensor and



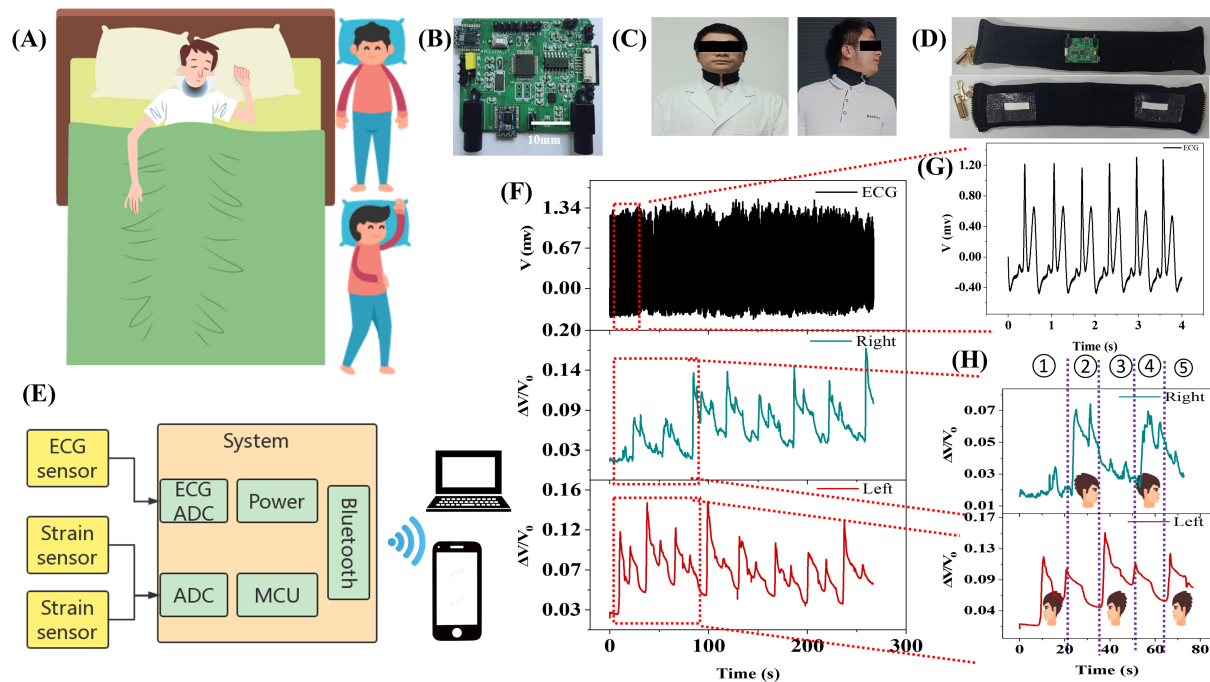


**Figure 5.** Sleep posture monitoring. (A) Illustration of sleep postures; (B) Photograph of the system circuit board; (C) Photograph of the system worn around the neck; (D) Photograph of the system; (E) Schematic diagram of the system architecture; (F) Signal plots of strain sensors and electrocardiogram during rotation in different directions during sleep; (G) Partial enlargement of ECG; (H) Partial enlargement of the strain sensor signal. ECG: Electrocardiogram; ADC: analog-to-digital converters; MCU: microcontroller unit.

strain sensors are individually routed to their respective analog-to-digital converters (ADCs) for signal conversion. Post-processing by a microcontroller unit (MCU), the signals are sent over Bluetooth to a mobile phone or PC. The system operates on a power source to supply the necessary energy.

Figure 5F–H shows the variations in strain sensor responses and ECG signal bilaterally when the wearable device is positioned around the neck in a supine position with the head turned either left or right. Observations indicate that turning the head to the left causes the left strain sensor to compress, leading to a notable strain and a correspondingly large voltage fluctuation. Likewise, turning the head to the right results in compression of the right strain sensor, causing considerable strain and a notable voltage alteration. Additionally, [Supplementary Figure 16](#) depicts the strain patterns for both strain sensors during continuous leftward head turns with the device in place around the neck, and [Supplementary Figure 17](#) presents the patterns during continuous rightward head turns in the same manner. The ECG signals maintain a high degree of stability throughout the head-turning process, demonstrating normal cardiac function. Should the head sustain a static position for an extended period during sleep, the strain sensor on the corresponding side will persistently show a certain degree of strain. Moreover, the occurrence of sleep-related breathing irregularities may result in noticeable variations in the ECG tracing or heart rate. These deviations can be swiftly identified via a smartphone, averting the onset of conditions like neck stiffness and sleep apnea. [Supplementary Figure 18](#) displays ECG recordings acquired by the system at 2-h intervals over an 8-h sleep period, utilized for assessing the heart's status throughout sleep. [Supplementary Figure 19](#) provides a comparison of the monitoring outcomes for head movement during sleep between our system and conventional video surveillance methods. Observations reveal that there was a single instance of erroneous judgment, demonstrating that the system possesses high monitoring precision.

## CONCLUSIONS

In this work, we present a high-performance and low-cost strain sensor using green solvent and printing techniques. The proposed graphene-CNTs-TPU/fabric strain sensor displayed a broad sensing range (0%-112%), high sensitivity ( $GF > 210$ ), an exceptionally low sensing limit ( $\sim 0.1\%$ ), outstanding response symmetry, and endurance through over 3,000 cycles. The sensor's operational performance and underlying mechanism were investigated from both macroscopic and microscopic viewpoints. When integrated with wireless test systems, the sensors find application in the realms of human exercise and healthcare monitoring. A sleep posture monitoring system has been engineered to monitor sleep positions, highlighting the promising application potential of this system within sleep monitoring.

## DECLARATIONS

### Authors' contributions

Conceptualization: He, P.; Yang, J.

Methodology, original draft preparation, and writing: Zhao, W.; Ling, K.; He, P.; Yang, J.

Provided administrative, technical, and material support: Gao, C.; Wang, K.; Wu, L.

Data analysis: Zhao, W.; Ling, K.

Conceptualization, funding acquisition, project administration, resources, supervision and writing, review and editing: He, P.; Yang, J.

### Availability of data and materials

The detailed characterizations and methods are available in the [Supplementary Materials](#). Other raw data that support the findings of this study are available from the corresponding author upon reasonable request.

### Financial support and sponsorship

This work was supported by the National Natural Science Foundation of China (52173192) and the National Key Research and Development Program of China (2022YFB3803300).

### Conflicts of interest

All authors declared that there are no conflicts of interest.

### Ethical approval and consent to participate

The study was conducted in accordance with the ethical guidelines and approved by the Medical Ethics Committee of Xiangya Stomatological Hospital, Central South University (No. 20240069). All participants were informed about the experimental procedure and signed the informed consent forms prior to participation.

### Consent for publication

Not applicable.

### Copyright

© The Author(s) 2025.

## REFERENCES

1. Rubin, S. E.; Wagner, R. S. Ocular torticollis. *Surv. Ophthalmol.* **1986**, *30*, 366-76. [DOI](#) [PubMed](#)
2. Zhu, H.; Liang, H.; Xiao, F.; Wang, G.; Hussain, R. Pressure image recognition of lying positions based on multi-feature value regularized extreme learning algorithm. *Appl. Math. Nonlinear. Sci.* **2023**, *8*, 559-72. [DOI](#)
3. Lee, J.; Hong, M.; Ryu, S. Sleep monitoring system using kinect sensor. *Int. J. Distrib. Sens. Netw.* **2015**, *2015*, 1-9. [DOI](#)
4. He, P.; Brent, J. R.; Ding, H.; et al. Fully printed high performance humidity sensors based on two-dimensional materials. *Nanoscale* **2018**, *10*, 5599-606. [DOI](#) [PubMed](#)

5. Amjadi, M.; Kyung, K.; Park, I.; Sitti, M. Stretchable, skin-mountable, and wearable strain sensors and their potential applications: a review. *Adv. Funct. Mater.* **2016**, *26*, 1678-98. DOI
6. Obitayo, W.; Liu, T. A review: carbon nanotube-based piezoresistive strain sensors. *J. Sens.* **2012**, *2012*, 1-15. DOI
7. Zhou, Z.; Chen, N.; Zhong, H.; et al. Textile-based mechanical sensors: a review. *Materials* **2021**, *14*, 6073. DOI PubMed PMC
8. Lv, G.; Wang, H.; Tong, Y.; et al. Flexible, conformable organic semiconductor proximity sensor array for electronic skin. *Adv. Mater. Interfaces.* **2020**, *7*, 2000306. DOI
9. Wei, P.; Yang, X.; Cao, Z.; et al. Flexible and stretchable electronic skin with high durability and shock resistance via embedded 3D printing technology for human activity monitoring and personal healthcare. *Adv. Mater. Technol.* **2019**, *4*, 1900315. DOI
10. Zhu, P.; Li, Z.; Pang, J.; He, P.; Zhang, S. Latest developments and trends in electronic skin devices. *Soft. Sci.* **2024**, *4*, 17. DOI
11. Miao, Y.; Xu, M.; Yu, J.; Zhang, L. Conductive cold-resistant and elastic hydrogel: a potential bionic skin for human-machine interaction control over artificial limbs. *Sens. Actuators. B. Chem.* **2021**, *327*, 128916. DOI
12. Wang, M.; Yan, Z.; Wang, T.; et al. Gesture recognition using a bioinspired learning architecture that integrates visual data with somatosensory data from stretchable sensors. *Nat. Electron.* **2020**, *3*, 563-70. DOI
13. Hu, M.; He, P.; Zhao, W.; et al. Machine learning-enabled intelligent gesture recognition and communication system using printed strain sensors. *ACS. Appl. Mater. Interfaces.* **2023**, Online ahead of print. DOI PubMed
14. Huang, J.; Guo, Y.; Jiang, Y.; Wang, F.; Pan, L.; Shi, Y. Recent advances and future prospects in tactile sensors for normal and shear force detection, decoupling, and applications. *J. Semicond.* **2024**, *45*, 121601. DOI
15. Clevenger, M.; Kim, H.; Song, H. W.; No, K.; Lee, S. Binder-free printed PEDOT wearable sensors on everyday fabrics using oxidative chemical vapor deposition. *Sci. Adv.* **2021**, *7*, eabj8958. DOI PubMed PMC
16. He, J.; Xiao, P.; Lu, W.; et al. A universal high accuracy wearable pulse monitoring system via high sensitivity and large linearity graphene pressure sensor. *Nano. Energy.* **2019**, *59*, 422-33. DOI
17. Yang, H.; Xiao, X.; Li, Z.; et al. Wireless  $\text{Ti}_3\text{C}_2\text{T}_x$  MXene strain sensor with ultrahigh sensitivity and designated working windows for soft exoskeletons. *ACS. Nano.* **2020**, *14*, 11860-75. DOI
18. Xu, X.; Li, Z.; Hu, M.; et al. High sensitivity and antifreeze silver nanowire/eutectic gel strain sensor for human motion and healthcare monitoring. *IEEE. Sensors. J.* **2024**, *24*, 5928-35. DOI
19. Jung, H. H.; Lee, H.; Yea, J.; Jang, K. Wearable electrochemical sensors for real-time monitoring in diabetes mellitus and associated complications. *Soft. Sci.* **2024**, *4*, 15. DOI
20. Choi, S.; Han, S. I.; Kim, D.; Hyeon, T.; Kim, D. H. High-performance stretchable conductive nanocomposites: materials, processes, and device applications. *Chem. Soc. Rev.* **2019**, *48*, 1566-95. DOI PubMed
21. Guo, D.; Pan, X.; He, H. Effects of temperature on MWCNTs/PDMS composites based flexible strain sensors. *J. Cent. South. Univ.* **2020**, *27*, 3202-12. DOI
22. Huang, X.; Qi, X.; Boey, F.; Zhang, H. Graphene-based composites. *Chem. Soc. Rev.* **2012**, *41*, 666-86. DOI PubMed
23. Zheng, Q.; Lee, J.; Shen, X.; Chen, X.; Kim, J. Graphene-based wearable piezoresistive physical sensors. *Mater. Today.* **2020**, *36*, 158-79. DOI
24. He, P.; Derby, B. Inkjet printing ultra-large graphene oxide flakes. *2D. Mater.* **2017**, *4*, 021021. DOI
25. Wu, L.; Li, Y.; Chen, J.; Zhang, R.; Zhang, Q.; Xiao, Y. Rare earth modified reduced graphene oxide reinforced AgCuTi composite brazing filler for brazing C/C composites. *J. Cent. South. Univ.* **2024**, *31*, 1398-411. DOI
26. Li, X.; Cai, W.; An, J.; et al. Large-area synthesis of high-quality and uniform graphene films on copper foils. *Science* **2009**, *324*, 1312-4. DOI PubMed
27. Deng, C.; Gao, P.; Lan, L.; et al. Ultrasensitive and highly stretchable multifunctional strain sensors with timbre-recognition ability based on vertical graphene. *Adv. Funct. Mater.* **2019**, *29*, 1907151. DOI
28. Huang, K.; Dong, S.; Yang, J.; et al. Three-dimensional printing of a tunable graphene-based elastomer for strain sensors with ultrahigh sensitivity. *Carbon* **2019**, *143*, 63-72. DOI
29. Wang, R.; Jiang, N.; Su, J.; et al. A Bi-Sheath fiber sensor for giant tensile and torsional displacements. *Adv. Funct. Materials.* **2017**, *27*, 1702134. DOI
30. Zeng, X.; Hu, M.; He, P.; et al. Highly conductive carbon-based E-textile for gesture recognition. *IEEE. Electron. Device. Lett.* **2023**, *44*, 825-8. DOI
31. Liu, Q.; Ramakrishna, S.; Long, Y. Electrospun flexible sensor. *J. Semicond.* **2019**, *40*, 111603. DOI
32. Seyedin, S.; Zhang, P.; Naebe, M.; et al. Textile strain sensors: a review of the fabrication technologies, performance evaluation and applications. *Mater. Horiz.* **2019**, *6*, 219-49. DOI
33. Huang, T.; He, P.; Wang, R.; et al. Porous fibers composed of polymer nanoball decorated graphene for wearable and highly sensitive strain sensors. *Adv. Funct. Mater.* **2019**, *29*, 1903732. DOI
34. Tian, X.; Chan, K.; Hua, T.; Niu, B.; Chen, S. Wearable strain sensors enabled by integrating one-dimensional polydopamine-enhanced graphene/polyurethane sensing fibers into textile structures. *J. Mater. Sci.* **2020**, *55*, 17266-83. DOI
35. Heo, J. S.; Shishavan, H. H.; Soleymampour, R.; Kim, J.; Kim, I. Textile-based stretchable and flexible glove sensor for monitoring upper extremity prosthesis functions. *IEEE. Sensors. J.* **2020**, *20*, 1754-60. DOI
36. Zhu, H.; Gao, H.; Zhao, H.; et al. Printable elastic silver nanowire-based conductor for washable electronic textiles. *Nano. Res.* **2020**, *13*, 2879-84. DOI
37. Luo, C.; Tian, B.; Liu, Q.; Feng, Y.; Wu, W. One-step-printed, highly sensitive, textile-based, tunable performance strain sensors for

- human motion detection. *Adv. Mater. Technol.* **2020**, *5*, 1900925. DOI
38. Shi, X.; Wang, H.; Xie, X.; et al. Bioinspired ultrasensitive and stretchable MXene-based strain sensor via nacre-mimetic microscale “brick-and-mortar” architecture. *ACS. Nano.* **2019**, *13*, 649-59. DOI PubMed
39. Tseghai, G. B.; Malengier, B.; Fante, K. A.; Nigusse, A. B.; Van, L. L. Development of a flex and stretchy conductive cotton fabric via flat screen printing of PEDOT:PSS/PDMS conductive polymer composite. *Sensors* **2020**, *20*, 1742. DOI PubMed PMC
40. He, Z.; Zhou, G.; Byun, J. H.; et al. Highly stretchable multi-walled carbon nanotube/thermoplastic polyurethane composite fibers for ultrasensitive, wearable strain sensors. *Nanoscale* **2019**, *11*, 5884-90. DOI PubMed
41. Yang, K.; Yin, F.; Xia, D.; Peng, H.; Yang, J.; Yuan, W. A highly flexible and multifunctional strain sensor based on a network-structured MXene/polyurethane mat with ultra-high sensitivity and a broad sensing range. *Nanoscale* **2019**, *11*, 9949-57. DOI PubMed
42. Xu, X.; Luo, M.; He, P.; Yang, J. Washable and flexible screen printed graphene electrode on textiles for wearable healthcare monitoring. *J. Phys. D.: Appl. Phys.* **2020**, *53*, 125402. DOI